



Journal of Applied and Computational Mechanics



Research Paper

Polymeric Dissipative Convection Flow from an Inclined Plane with Chemical Reaction: Numerical Study

Santhosh Madhavi¹, V. Ramachandra Prasad², Shaik Abdul Gaffar³

¹ Madanapalle Institute of Technology and Science, Department of Mathematics, Madanapalle, 517325, India, Email: santhoshmadhavi3@gmail.com

² School of Advanced Sciences, Vellore Institute of Technology, Department of Mathematics, Vellore, 632014, India, Email: rcpmaths@gmail.com

³ Salalah College of Technology, Department of Information Technology, Mathematics Section, Salalah, 211, Oman, Email: sa.gaffar@sct.edu.om

Received August 16 2019; Revised December 18 2019; Accepted for publication December 26 2016.

Corresponding author: S. Abdul Gaffar (abdulsgaffar0905@gmail.com)

© 2020 Published by Shahid Chamran University of Ahvaz

Abstract. An analytical model is developed to study the effects of viscous dissipation and chemical reaction in viscoelastic convection from an inclined plate as a simulation of electro-conductive polymer materials processing. The Jeffery's viscoelastic model is deployed to describe the non-Newtonian characteristics of the fluid and provides a good approximation for polymers, which constitutes a novelty of the present work. The normalized nonlinear boundary value problem is solved computationally with the Keller-Box implicit finite-difference technique. Extensive solutions for velocity, surface temperature and concentration, skin friction, heat, and transfer rates are visualized numerically and graphically for various thermophysical parameters. Validation is conducted with earlier published work for the case of a vertical plate in the absence of viscous dissipation, chemical reaction, and non-Newtonian effects. The boundary layer flow is accelerated with increasing Deborah number whereas temperatures and concentrations are decelerated slightly. Temperatures and concentration are boosted with increasing inclination parameter whereas velocity is lowered. A reverse trend is seen for increasing Richardson number. Increasing chemical reaction reduces velocity and concentration whereas it enhances temperature. Increasing the viscous dissipation parameter is found to enhance velocity and temperature whereas it suppresses concentration.

Keywords: Viscoelastic fluid; Inclined plate; Chemical reaction; Viscous dissipation; Retardation time.

1. Introduction

In nature, we periodically come across the laminar convection flows which have several applications in science and technology. Natural convection along an inclined plate has received less attention than the classic case of vertical and horizontal plates. However, natural convection heat transfer from an inclined surface is encountered frequently in engineering devices and the natural environment. Extensive research has been carried out on the flows past the inclined plate. The transport phenomena along an inclined surface arise in many applications in industry such as fuel combustion [1], condensation systems [2], magnetic thin film deposition [3], geophysical debris flows [4], thermal coating [5] and geothermal heat transfer from oblique faults [6]. In materials processing systems, the use of an inclined plane allows the thermal buoyancy force to easily modify as it is proportional to the inclination angle. Materials manufacturing operations (e.g. plastic coating dynamics [7], gel and thin-film systems [8]) also feature non-Newtonian fluids. The rheology of the involved fluids significantly modifies momentum and heat transfer characteristics in such flows. In the context of thermoplastic sheet processing, viscoelastic film flows may become unstable due to fluid elasticity which is controlled by the Weissenberg number [9]. Many rheological models have subsequently been deployed in recent years to



study thermal and momentum boundary-layer flows from inclined surfaces. These studies have also utilized many advanced numerical methods that are required to accommodate the nonlinearity of such flows. Roy *et al.* [10] analysed the variations of sinusoidal surface temperature on the combustible boundary layer flows past a hot inclined surface. They observed a significant increase in heat and mass transfer boundary layer with an increase in the angle of inclination. Sulochana *et al.* [11] presented the MHD flow of Casson nanofluid past a semi-infinite inclined porous plate with chemical reaction using the perturbation technique. They observed that the radiation and chemical reaction parameters accelerate both heat and mass transfer rates. Hayat *et al.* [12] explored the non-Fourier's heat flux model flow characteristics of Eyring-Powell fluid with variable thermal conductivity considering the stagnation point flow. They observed that the temperature for the Cattaneo-Christov heat flux model is less than the Fourier's expression. Hayat *et al.* [13] investigated the stagnation point flow of Maxwell fluid over a stretching cylinder. They observed that the temperature profiles decay for higher values of thermal relaxation parameter. Ijaz *et al.* [14] addressed the MHD stagnation point flow of Casson fluid towards a stretching sheet. They considered the Homogeneous-heterogeneous reactions together with homogeneous heat effect. Few recent studies include power-law fluid flows [15 – 16] and micropolar fluid flows [17]. The non-Newtonian nature of waste products has been observed in different studies. Polymeric flows are generally non-Newtonian in nature. In coating applications, heat transfer plays a vital role in determining the constitution of manufactured polymers. In dip coating processes, the surface is first immersed in a polymer and then steadily withdrawn. As polymers have high viscosity, industrial chemical or manufacturing flow processes exploiting such fluids are generally laminar in nature. The rheological nature of polymers also necessitates more sophisticated mathematical models for describing shear stress-strain relationships. Among the many viscoelastic fluids available, the Jeffrey model [18] has emerged as a good approximation for polymer dynamics. This model features three constants, namely the zero shear-rate viscosity, ratio of relaxation and retardation time and the retardation time. The Jeffrey's fluid model describes the characteristics of relaxation and retardation times which arise in complex polymeric flows. The Jeffrey's model provides an elegant formulation for simulating elastic effects that arise in non-Newtonian flows. It is appropriate for nonlinear viscoelastic effects for which the simpler inelastic models cannot be used. Jeffrey's model is obtained by adding a time derivative of the shear rate to the conventional Maxwell linear model. The convected Jeffrey model (Oldroyd model) also allows several other special cases to be obtained. When retardation time is neglected the original Maxwell model is retrieved. When the relaxation time is neglected then the case of a second-order differential fluid is obtained for which the normal stress coefficient is zero. Finally, when both relaxation and retardation times are equivalent then the Newtonian fluid case is obtained. Jeffrey's model was used by Prasad *et al.* [19] to study the steady-state thermal polymer coating flow of a plate in porous media. Gaffar *et al.* [20] investigated the non-isothermal and non-isolutal transport phenomena from a porous conical body using the Jeffrey model. These studies all showed how significant modifications are computed in heat, flow and species diffusion fields due to viscoelastic material behavior. Kumar *et al.* [21] studied the unsteady hydromagnetic flow of a Jeffrey fluid from a vertical surface using a Crank-Nicholson difference method. They showed that increasing Jeffrey fluid parameters (relaxation and retardation parameters) enhance the entropy generation number whereas the contrary effect is induced with stronger magnetic field.

The boundary layer flows with chemical reaction has gained considerable importance due to its applications in various chemical and hydrometallurgical industries. Many practical diffusive operations involve the molecular diffusion of a species in the presence of chemical reaction within or at the boundary. The chemical reaction can be systematized as either heterogeneous or homogeneous procedures that depend on whether it occurs on an interface or a single-phase volume reaction. The heterogeneous reaction occurs in a single phase whereas the homogeneous reaction occurs uniformly in a given phase. In a first-order reaction, the rate of reaction is directly proportional to concentration. The chemical reaction is due to the presence of a foreign mass in the fluid. The presence of a chemical reaction is by itself or as a mixture with the fluid. In chemical engineering processes, such as polymer production, ceramics or glassware manufacturing, and food processing, a chemical reaction occurs between the foreign mass and the fluid. Many rheological models have subsequently been deployed in recent years to study the effects of the chemical reaction. Shukla *et al.* [22] studied the influence of radiative flux on entropy generation in transient magnetized nano-polymer stagnation flow with chemical reaction effects. Khan *et al.* [23] showed that radiative flux enhances temperatures and reduces entropy generation in magnetic nanofluid flow with binary chemical reaction. Mondal *et al.* [24] presented the thermophoresis and sores-Dufour effects on 2c mixed convection flows using the RKF45 method using shooting technique. Krishnamurthy *et al.* [25] analyzed the chemical reaction and melting heat transfer effects on MHD convection flows of Williamson nanofluid in the porous medium. Ramana *et al.* [26] numerically studied the chemical reaction effects on MHD nanofluid flows past a vertically moving flat plate in porous media using the perturbation technique. Ijaz *et al.* [27] presented the concept of activation energy in mixed convective MHD stagnation point flow towards the stretching surface with chemical reaction effects on the surface. They also considered the nanofluid for thermophoresis and Brownian effects along with nonlinear thermal radiation and heat generation/absorption effects. They observed that the species concentration will enhance for greater activation energy variable.

The impact of viscous dissipation emerges in numerous modern industrial and geophysical streams due to the internal friction in viscous fluids that influence temperature fields. The presence of viscous dissipation increases the motion of the fluid as it converts kinetic energy into internal energy which results in heating up the fluid. The transaction between the fluid rheology and viscous dissipation offers ascend to a huge modification in the net convective transport and subsequently benefit the thermal structure of biofluidic gadgets. Numerous studies involving the effects of



viscous heating have been reported. Hayat *et al.* [28] explored the mixed convective flow of viscous fluid in a nonlinear stretching rotating disk with thermal radiation, Joule heating, and viscous dissipation. Hayat *et al.* [29] examined the viscous dissipation and Joule heating effects in an MHD radiative flow by a rotating disk of variable thickness. They observed that the entropy generation rate decreases with an increase in Hartmann number, Eckert number and Reynolds number whereas the Bejan number increases. Khan *et al.* [30] discussed the entropy generation of nonlinear radiative nanomaterial flow over a thin moving needle with viscous dissipation. They observed that for the greater radiative parameter the heat transfer rate is lowered. Hayat *et al.* [31] discussed the impact of Joule heating and viscous dissipation in radiative nanoparticle fluid flow from a stretching cylinder. They employed Euler's Explicit method to solve the nonlinear differential system. They observed that the velocity of the fluid decays with increasing magnetic parameter. Ijaz *et al.* [32] employed the shooting technique to discuss the Darcy Forchheimer dissipative nonlinear radiative flow of viscous fluid from a nonlinear stretching surface with Joule heating and homogeneous-heterogeneous reactions. They noticed that the increasing Hartmann number decreases the velocity however the thermal and concentration profiles are enhanced for higher Eckert and Biot numbers. Hayat *et al.* [33] investigated the melting heat transfer in the squeezing flow of carbon nanotubes over a Riga plate with viscous dissipation. They employed the shooting technique. They observed that the temperature distributions reduce due to higher values of melting parameter and nanoparticle volume fraction. Ijaz *et al.* [34] analysed the entropy and Bejan numbers in MHD nonlinear radiative and mixed convection tangent hyperbolic nanofluid flows past the stretching sheet in the presence of Joule heating, chemical reaction and viscous dissipation. They found that for higher chemical reaction values the concentration is lowered. Also, they observed that the entropy number is higher for higher Hartmann number, Weissenberg number, and chemical reaction. Recent studies include Abdul Gaffar *et al.* [35 – 37].

In recent years new sophisticated *polymers* have emerged which provide enhanced performance in many industrial sectors including aerospace, manufacturing, energy and medical engineering. These include magnetoelectric nanocomposites [38] and soft magnetic polymer gels [39]. These materials are frequently synthesized at high temperature. The current study, therefore, aims to simulate the transport phenomena in the flow of such materials along an inclined surface in the presence of chemical reaction and viscous dissipation effects. The Jeffrey rheological model is deployed for non-Newtonian behaviour. The emerging non-dimensional nonlinear boundary value problem is solved with the Keller box implicit finite difference method [40]. Verification of the computations is included via comparison with earlier studies. Extensive visualization via graphs of the influence of key parameters (*Deborah viscoelastic parameter, ratio of relaxation to retardation parameter, chemical reaction parameter, viscous dissipation parameter, etc.*) on velocity, temperature, skin friction, heat and mass transfer rate characteristics is included. The present problem to the authors' knowledge has thus far not been considered in the scientific literature and constitutes a novel effort in thermodynamic analysis of magnetic non-Newtonian materials processing operations.

2. Mathematical Model

Natural convection in laminar, two-dimensional, time-independent incompressible Jeffrey viscoelastic polymer flow [41 - 42] from an inclined rigid sheet is considered, as illustrated in Fig. 1.

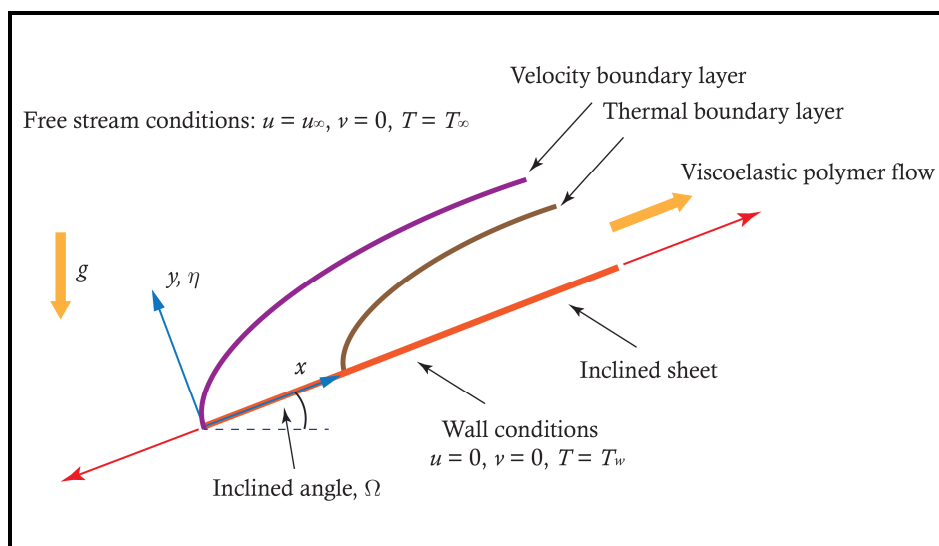


Fig. 1. Physical model for inclined plane flow

The sheet is inclined at an angle, Ω , to the horizontal. The polymer is assumed to be an optically dense, absorbing but non-scattering fluent medium. In this model, with the exception of the density variation in the buoyancy terms (Boussinesq approximation) all other properties are assumed to be constant. To simulate non-Newtonian characteristics of the Jeffery elastic-viscous fluid model, the Cauchy stress tensor is required which is defined as [18-21, 42]:



$$T = -pI + S, \quad S = \frac{\mu}{1 + \lambda} \left(\dot{\gamma} + \lambda_1 \ddot{\gamma} \right) \tag{1}$$

$$\dot{\gamma} = \nabla V + (\nabla V)^t \tag{2}$$

$$\ddot{\gamma} = \frac{d}{dt} \left(\dot{\gamma} \right) \tag{3}$$

Here, $p, I, S, \mu, \lambda, \lambda_1$ and $\dot{\gamma}$, denote pressure, identity tensor, Cauchy stress tensor for *Jeffery fluid*, viscosity, ratio of relaxation to retardation time, retardation time and shear rate. The Jeffery model therefore features three constants i.e. viscosity at zero shear rate and two time-related material parameter constants. Incorporating the appropriate terms under the boundary-layer approximation, the following conservation equations emerge for mass, momentum, energy (heat) and concentration:

$$\frac{\partial u}{\partial x} + \frac{\partial v}{\partial y} = 0 \tag{4}$$

$$u \frac{\partial u}{\partial x} + v \frac{\partial u}{\partial y} = \frac{\nu}{1 + \lambda} \left(\frac{\partial^2 u}{\partial y^2} + \lambda_1 \left[u \frac{\partial^3 u}{\partial x \partial y^2} - \frac{\partial u}{\partial x} \frac{\partial^2 u}{\partial y^2} + \frac{\partial u}{\partial y} \frac{\partial^2 u}{\partial x \partial y} + v \frac{\partial^3 u}{\partial y^3} \right] \right) + g[\beta(T - T_\infty) + \beta^*(C - C_\infty)] \cos \Omega \tag{5}$$

$$u \frac{\partial T}{\partial x} + v \frac{\partial T}{\partial y} = \frac{k}{\rho c_p} \frac{\partial^2 T}{\partial y^2} + \frac{\nu}{c_p} \left(\frac{\partial u}{\partial y} \right)^2 \tag{6}$$

$$u \frac{\partial C}{\partial x} + v \frac{\partial C}{\partial y} = D_m \frac{\partial^2 C}{\partial y^2} - K_1(C - C_\infty) \tag{7}$$

The relevant boundary conditions imposed at the plate surface and in the free stream:

$$\begin{aligned} \text{at } y = 0, \quad & u = 0, \quad v = 0, \quad T = T_w, \quad C = C_w \\ \text{when } y \rightarrow \infty, \quad & u \rightarrow u_\infty, \quad v \rightarrow 0, \quad T \rightarrow T_\infty, \quad C \rightarrow C_\infty \end{aligned} \tag{8}$$

The nonlinearity of the conservation equations in primitive variables makes even a numerical solution difficult. It is judicious therefore to reduce the number of independent variables and to this end the following group of variables is invoked:

$$\begin{aligned} \xi = \frac{x}{L}, \quad \eta = y \left(\frac{u_\infty}{\nu x} \right)^{1/2}, \quad \psi = (\nu u_\infty x)^{1/2} f, \quad De = \frac{\lambda_1 \nu Re_x}{x^2}, \quad Re_x = \frac{u_\infty x}{\nu}, \quad Re = \frac{u_\infty L}{\nu}, \quad Sc = \frac{\nu}{D_m}, \quad Pr = \frac{\nu \rho c_p}{k} \\ \theta(\xi, \eta) = \frac{T - T_\infty}{T_w - T_\infty}, \quad \phi(\xi, \eta) = \frac{C - C_\infty}{C_w - C_\infty}, \quad Gr = \frac{g\beta(T_w - T_\infty)L^3}{\nu^2}, \quad Ri = \frac{Gr}{Re^2}, \quad Ec = \frac{U_\infty^2}{c_p(T_w - T_\infty)}, \quad Kr = \frac{LK_1}{U_\infty} \end{aligned} \tag{9}$$

Incorporating Eqn. (9) into Eqns. (4) - (7), the continuity equation (4) is automatically satisfied and the emerging non-dimensional momentum and thermal boundary layer equations emerge as:

$$\frac{f'''}{1 + \lambda} + \frac{1}{2} f f'' + R\xi(\theta + N\phi) \cos \Omega - \frac{De}{1 + \lambda} \left(\frac{1}{2} f''^2 + f' f''' + \frac{1}{2} f f^{iv} \right) = \xi \left(f' \frac{\partial f'}{\partial \xi} - f'' \frac{\partial f}{\partial \xi} - \frac{De}{1 + \lambda} \left(f' \frac{\partial f'''}{\partial \xi} - f''' \frac{\partial f'}{\partial \xi} + f'' \frac{\partial f''}{\partial \xi} - f^{iv} \frac{\partial f}{\partial \xi} \right) \right) \tag{10}$$

$$\frac{\theta''}{Pr} + \frac{1}{2} f \theta' + Ec(f'')^2 = \xi \left(f' \frac{\partial \theta}{\partial \xi} - \theta' \frac{\partial f}{\partial \xi} \right) \tag{11}$$

$$\frac{\phi''}{Sc} + \frac{1}{2} f \phi' - Kr\xi\phi = \xi \left(f' \frac{\partial \phi}{\partial \xi} - \phi' \frac{\partial f}{\partial \xi} \right) \tag{12}$$

The transformed dimensionless wall and free stream boundary conditions assume the form:



$$\begin{aligned} &\text{at } \eta = 0, & f = 0, & f' = 0, & \theta = 1, & \phi = 1 \\ &\text{when } \eta \rightarrow \infty, & f' \rightarrow 1, & f'' \rightarrow 0, & \theta \rightarrow 0, & \phi \rightarrow 0 \end{aligned} \tag{13}$$

Additionally, the dimensionless expressions for the physical quantities at the plate surface can be written as:

$$\sqrt{\text{Re}_x} C_f = \frac{1}{1+\lambda} \left(f''(\xi, 0) - \frac{De}{2} (f'(\xi, 0) * f''(\xi, 0) + f(\xi, 0) * f'''(\xi, 0)) \right) \tag{14}$$

$$\frac{Nu}{\sqrt{\text{Re}_x}} = -\theta'(\xi, 0) \tag{15}$$

$$\frac{Sh}{\sqrt{\text{Re}_x}} = -\phi'(\xi, 0) \tag{16}$$

Here the expressions $\sqrt{\text{Re}_x} C_f, Nu / \sqrt{\text{Re}_x}$ and $Sh / \sqrt{\text{Re}_x}$ denote skin friction coefficient (wall shear stress function), local Nusselt number (wall heat transfer rate) and local Sherwood number (wall mass transfer rate) respectively.

3. Numerical Finite Difference Solutions

The boundary value problem to be solved comprises Eqns. (10) - (12) under boundary conditions (13). The Keller box method is selected to obtain numerical solutions. This method is well-documented in many studies [43 – 44] and details are therefore omitted here. To validate the Keller box numerical code employed, comparison with earlier Newtonian solutions presented by Lloyd and Sparrow [45] is conducted and shown in Table 1. Very close correlation is achieved for the Nusselt number (*Nu*) for different values of the Richardson number (*Ri*) and three different values of Prandtl number (*Pr*) i.e. 0.72 (air), 10, 100 (polymers). Confidence in the present solutions is therefore very high.

Table 1. Comparison values of *Nu* for different values of *R* and *Pr*.

<i>R</i>	<i>Pr</i> = 0.72		<i>Pr</i> = 10		<i>Pr</i> = 100	
	Lloyd and Sparrow [45]	Present	Lloyd and Sparrow [45]	Present	Lloyd and Sparrow [45]	Present
0.0	0.2956	0.2958	0.7281	0.7283	1.5720	1.5724
0.01	0.2979	0.2980	0.7313	0.7315	1.5750	1.5753
0.04	0.3044	0.3046	0.7404	0.7406	1.5850	1.5851
0.1	0.3158	0.3160	0.7574	0.7576	1.6050	1.6052
0.4	0.3561	0.3563	0.8259	0.8261	1.6910	1.6912
1.0	0.4058	0.4060	0.9212	0.9213	1.8260	1.8262

Table 2. Values of *C_f*, *Nu* and *Sh* for various values of *De*, λ and Ω (*Pr* = 7, *R* = 0.5, *Ec* = 0.1, *Kr* = 0.5, *Sc* = 0.6, *N* = 0.5, ξ = 1.0)

<i>De</i>	λ	$\Omega = 0$			$\Omega = \pi/6$			$\Omega = \pi/3$			$\Omega = \pi/2$		
		<i>C_f</i>	<i>Nu</i>	<i>Sh</i>									
0.01		0.7828	0.7033	0.5774	0.7263	0.6957	0.5733	0.5446	0.6640	0.5618	0.2692	0.5726	0.5065
	1	0.7845	0.6938	0.5754	0.7272	0.6854	0.5710	0.5497	0.6574	0.5610	0.2761	0.5717	0.5044
	2	0.7897	0.6842	0.5740	0.7277	0.6781	0.5704	0.5542	0.6510	0.5608	0.2838	0.5719	0.5024
	3	0.7920	0.6734	0.5734	0.7286	0.6676	0.5702	0.5582	0.6439	0.5605	0.2926	0.5716	0.5006
	4	0.7923	0.6585	0.5730	0.7290	0.6539	0.5544	0.5653	0.6338	0.5604	0.3030	0.5688	0.4987
	0	0.8368	0.7003	0.5729	0.7780	0.6913	0.5691	0.6070	0.6565	0.5574	0.3308	0.5642	0.4970
	0.5	0.7166	0.6996	0.5827	0.6649	0.6944	0.5785	0.5143	0.6686	0.5652	0.2701	0.5812	0.5014
0.1	1	0.6411	0.6853	0.5899	0.5939	0.6843	0.5854	0.4569	0.6688	0.5710	0.2339	0.5898	0.5050
	1.5	0.5875	0.6641	0.5955	0.5437	0.6675	0.5907	0.4165	0.6628	0.5757	0.2092	0.5940	0.5079
	2	0.5467	0.6388	0.6000	0.5056	0.6466	0.5951	0.3860	0.6531	0.5795	0.1910	0.5954	0.5104

4. Results and Discussion

Table 2 presents the numerical results of dimensionless skin friction (*C_f*), heat transfer rate (*Nu*) and mass transfer rate (*Sh*) for different values of Deborah number *De* and ratio of retardation to relaxation times, λ along with variations in inclination angle, Ω . An increasing *De* is observed to increase *C_f* whereas it decreases both *Nu* and *Sh*. Furthermore, an increase in λ reduces the skin friction and heat transfer rate but enhances the mass transfer rate. The raise in λ physically implies a reduction in fluid retardation time. However, an increase in Ω is seen to reduce skin friction, heat and mass transfer rates.



Table 3. Values of C_f , Nu and Sh for various values of Kr , Ec and R ($Pr = 7$, $De = 0.1$, $\lambda = 0.2$, $\Omega = \pi/6$, $Sc = 0.6$, $N = 0.5$)

Kr	Ec	R	$\xi = 1.0$			$\xi = 2.0$			$\xi = 3.0$		
			C_f	Nu	Sh	C_f	Nu	Sh	C_f	Nu	Sh
-10			3.2052	0.4186	-74.1179	16.3184	-11.3085	-400.38	42.0471	-54.265	-951.754
-5			1.1746	0.6721	-8.3864	3.7655	0.1240	-43.0459	9.0851	-3.6528	-111.871
0	0.1	0.5	0.7381	0.6783	0.3482	1.0762	0.7222	0.3824	1.3793	0.7096	0.4077
5			0.6665	0.6984	1.7396	0.9240	0.7050	2.4615	1.1502	0.7101	3.0119
10			0.6432	0.7720	2.4598	0.8892	0.7018	3.4785	1.1068	0.7103	4.2571
		0	0.7116	0.8782	0.5718	1.0153	0.9873	0.7729	1.2792	1.0650	0.9392
		0.5	0.7794	-0.1338	0.5788	1.1410	-0.5609	0.7803	1.4649	-1.0402	0.9464
0.5	1	0.5	0.8482	-1.3922	0.5853	1.2729	-2.6565	0.7873	1.6655	-4.0648	0.9536
		1.5	0.9181	-2.9122	0.5914	1.4108	-5.3647	0.7940	1.8807	-8.1655	0.9607
		2	0.9892	-4.7095	0.5972	1.5547	-8.7542	0.8005	2.1104	-13.511	0.9677
		0	0.3020	0.5724	0.4989	0.3020	0.5724	0.6874	0.3020	0.5724	0.8552
		0.25	0.5319	0.6554	0.5582	0.7107	0.6804	0.7604	0.8677	0.5878	0.9290
0.5	0.1	0.5	0.7251	0.6948	0.5733	1.0400	0.6910	0.7744	1.3151	0.6638	0.9406
		0.71	0.8995	0.7139	0.5853	1.3353	0.7184	0.7858	1.7168	0.7082	0.9504
		1	1.0619	0.7204	0.5956	1.6102	0.7101	0.7956	2.0917	0.7104	0.9591

Table 4. Values of C_f , Nu and Sh for various values of Pr , Sc and N ($R = 0.5$, $De = 0.1$, $\lambda = 0.2$, $\Omega = \pi/6$, $Kr = 0.6$, $Ec = 0.1$)

Pr	Sc	N	$\xi = 1.0$			$\xi = 2.0$			$\xi = 3.0$		
			C_f	Nu	Sh	C_f	Nu	Sh	C_f	Nu	Sh
0.5			0.8415	0.3214	0.5901	1.2450	0.3472	0.7924	1.6009	0.3614	0.9575
0.71			0.8271	0.3628	0.5878	1.2192	0.3912	0.7898	1.5647	0.4062	0.9550
1			0.8122	0.4063	0.5855	1.1928	0.4371	0.7873	1.5277	0.4522	0.9526
2	0.6	0.5	0.7810	0.5026	0.5808	1.1376	0.5362	0.7823	1.4505	0.5492	0.9479
3			0.7625	0.5631	0.5782	1.1051	0.5964	0.7795	1.4053	0.6058	0.9453
5			0.7400	0.6423	0.5751	1.0652	0.6715	0.7763	1.3499	0.6724	0.9424
	0.25		0.7455	0.6997	0.3820	1.0791	0.7206	0.5063	1.3725	0.7129	0.6106
	0.75		0.7192	0.6934	0.6368	1.0289	0.7177	0.8640	1.2991	0.7126	1.0510
7.0	0.98	0.5	0.7119	0.6915	0.7226	1.0153	0.7166	0.9855	1.2796	0.7118	1.2008
	1.25		0.6999	0.6885	0.8842	0.9931	0.7147	1.2157	1.2482	0.7111	1.4850
	1.5		0.6916	0.6863	1.0142	0.9780	0.7132	1.4017	1.2270	0.7067	1.7148
		-0.5	0.4013	0.6051	0.5420	0.5107	0.6389	0.7493	0.6229	0.6676	0.9245
		-0.25	0.4883	0.6375	0.5512	0.6515	0.6756	0.7559	0.8039	0.6993	0.9277
7.0	0.6	0	0.5706	0.6619	0.5592	0.7859	0.6990	0.7624	0.9795	0.7148	0.9318
		0.25	0.6493	0.6806	0.5665	0.9151	0.7126	0.7685	1.1497	0.7177	0.9362
		0.75	0.7984	0.7054	0.5795	1.1611	0.7181	0.7800	1.4762	0.6948	0.9451

Table 3 document results for the influence of *chemical reaction parameter* (Kr), *Eckert number* (Ec) and *Richardson number* (Ri) on dimensionless skin friction, heat and mass transfer rates along with a variation in the traverse coordinate (ξ). Skin friction is reduced with increasing Kr values however both heat and mass transfer rates are enhanced. Furthermore, the increasing values of Ec are seen to increase skin friction and mass transfer rate whereas the heat transfer rate decreases. Whereas, increasing Ri is seen to enhance skin friction, heat and mass transfer rate.

Table 4 presents the variations of skin friction, heat and mass transfer rate for various values of Prandtl number, Pr , Schmidt number, Sc and Buoyancy ratio parameter N along with a variation in the traverse coordinate (ξ). An increasing Pr depresses the skin friction and mass transfer rate whereas elevates the heat transfer rate. In order to generalise the solutions to denser fluids i.e., water-based solvents, very low-density spray paints, etc., Pr is to be varied. For example, $Pr = 5$ corresponds to actual characteristics of chlorofluorocarbon halomethane (CFC) which is used in aerosol spray propellants. $Pr = 7$ represents paint thinners. Pr is the ratio of viscous diffusion to thermal diffusion in the boundary layer regime. For $Pr > 1$ momentum diffusion exceeds thermal diffusion and for $Pr > 1$ thermal diffusion exceeds momentum diffusion. Greater Pr reduces velocity and hence reduces C_f . Therefore, the corresponding momentum boundary layer thickness increases. Greater Pr values correspond to thinner thermal boundary layer thickness and more uniform temperature distributions across the boundary layer. $Pr = 0.71$ corresponds to fluids with higher thermal conductivity. And $Pr = 7.0$ corresponds to fluids with thinner boundary layers. An increasing Sc depresses the skin friction and heat transfer rate whereas boosts the mass transfer rate. For $Sc > 1$, the momentum diffusion rate exceeds the species diffusion rate whereas for $Sc < 1$, species diffusion rate exceeds the momentum diffusion rate. And for $Sc = 1$ both species and momentum diffusion rates are the same and the momentum and concentration boundary layer thicknesses equal in the regime. An increasing N elevates the skin friction, heat and mass transfer rates.



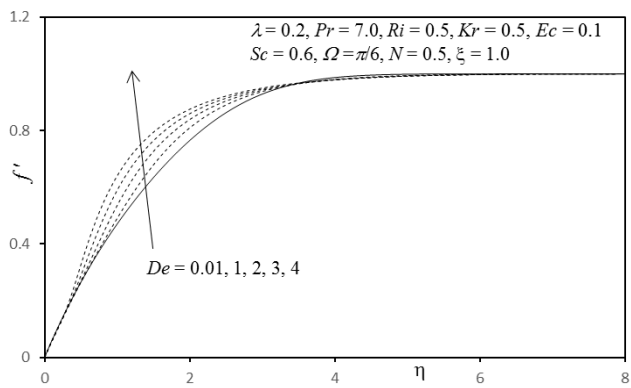


Fig. 2. Influence of De on Velocity Profiles

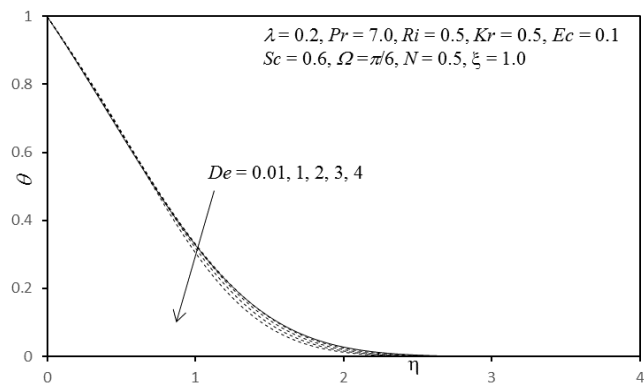


Fig. 3. Influence of De on Temperature Profiles

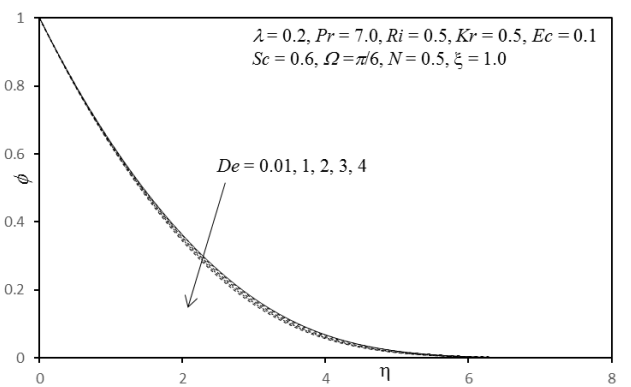


Fig. 4. Influence of De on Concentration Profiles

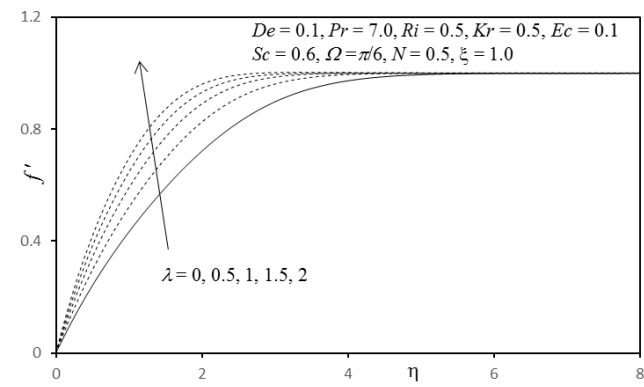


Fig. 5. Influence of λ on Velocity Profiles

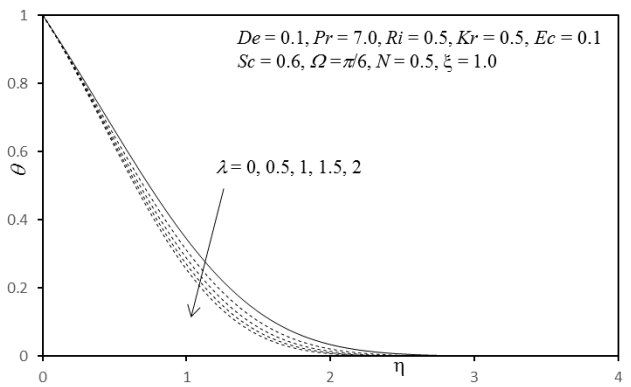


Fig. 6. Influence of λ on Temperature Profiles

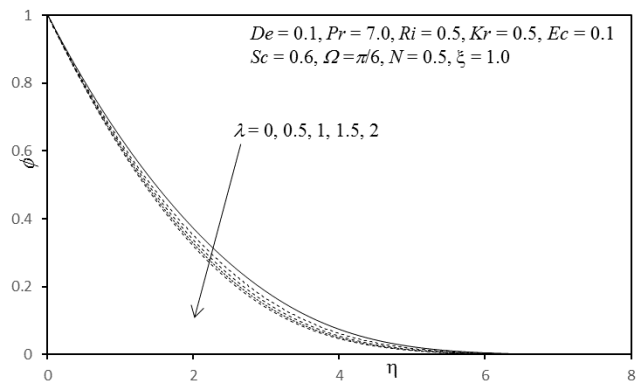


Fig. 7. Influence of λ on Concentration Profiles

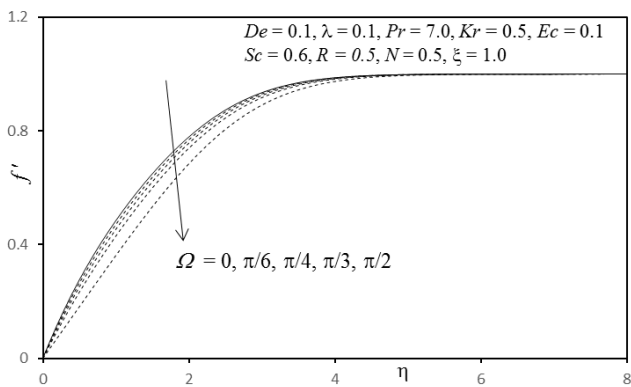


Fig. 8. Influence of Ω on Velocity Profiles

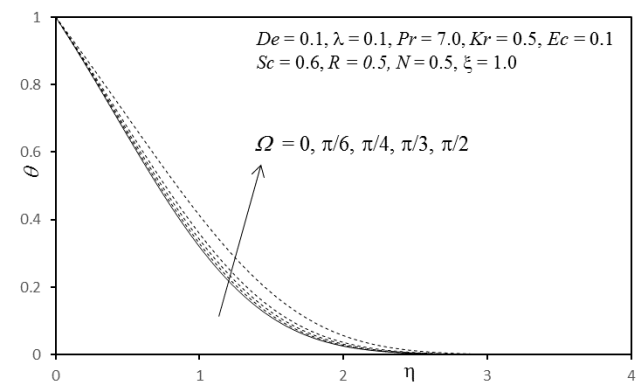


Fig. 9. Influence of Ω on Temperature Profiles



Figures 2 to 19 illustrate graphical solutions for the influence of selected parameters on the velocity, temperature, concentration, skin friction, heat and mass transfer rate characteristics. Figures 2 to 4 depict the influence of Deborah number (viscoelastic parameter) on velocity, temperature, and concentration (f' , θ and ϕ). In all graphs, plate inclination is set at $\Omega = \pi/6$. Asymptotically smooth distributions are generally achieved in the freestream for all graphs indicating that a sufficiently large infinity boundary condition is specified in the Keller box numerical code. Fig. 2 shows the influence of De on f' and clearly increasing De (which corresponds to greater elastic effects to viscous effects) results in flow acceleration. De embodies the ratio of relaxation time it takes for the fluid to adjust to applied stresses or deformations and the characteristic time scale. Momentum boundary layer thickness is therefore reduced with increasing Deborah number. The fluid (polymer) behaves more like a viscous fluid at lower Deborah number whereas, at higher Deborah numbers, the behaviour is more influenced by elasticity. Fig. 3 demonstrates that increasing De values result in a decrease in temperature i.e. reduction in thermal boundary layer thickness. The effect of De on the concentration is shown in Fig. 4 and a very slight decrease is observed.

Figures 5 to 7 show the response of fluid velocity (f'), temperature (θ), and concentration (ϕ) with the ratio of relaxation to retardation times (λ). A significant elevation in velocity accompanies an increase in λ as observed in Fig. 5. Conversely, there is a strong reduction in temperature with increasing λ values (Fig. 6). Fig. 7 shows that concentration is slightly reduced with increasing values of the ratio of relaxation to retardation times (λ). Effectively the rheology of Jeffery fluid has a marked influence on thermal and hydrodynamic characteristics. For the case of a Newtonian fluid ($\lambda = 1$), the results are noticeably different from the Jeffery case ($\lambda \neq 1$). When $\lambda < 1$, the retardation time exceeds the relaxation time. This implies that the polymeric Jeffrey fluid responds faster with the removal of stress and returns quicker to its unperturbed state. The opposite behaviour is the case when $\lambda > 1$.

Figures 8 to 10 show the distributions for velocity (f'), fluid temperature (θ), and concentration (ϕ) with the angle of inclination (Ω) varying between 0° to 90° . Fig. 8 indicates that a significant deceleration in the boundary layer flow is associated with Ω which is due to the reduction in the thermal buoyancy effect in Eqn. (5). From fig. 8 we also observe for $\Omega = 0^\circ$ (vertical plate) the temperature and concentration attain maximum buoyancy force. The increasing angle of inclination parameter (Ω) is observed in Fig. 9 to elevate the fluid temperature (θ) and enhances thermal boundary layer thickness. Fig. 10 shows that concentration profiles are slightly elevated with increasing inclination parameter. i.e. for the vertical surface, we observe that the temperature and concentration distributions are small but for the horizontal surface, they are large.

Figures 11 to 13 visualize the response in fluid velocity (f'), Jeffery fluid temperature (θ), and concentration (ϕ) to a variation in Richardson number (Ri). Larger values of Ri correspond to stronger natural (free) convection i.e. greater Grashof numbers. A significant elevation in velocity is induced throughout the boundary layer transverse to the plate surface with increasing Ri , as seen in Fig. 11. Momentum boundary layer thickness is therefore decreased. Temperatures are considerably depleted (Fig. 12) with greater Ri values i.e. thermal boundary layer thickness is reduced. In both Figs. 11 and 12 the trends are sustained throughout the boundary layer. Fig. 13 shows that in close proximity to the plate surface there is a significant decrease in concentration with a rise in Richardson number.

Figures 14 to 16 show the distributions for velocity (f'), fluid temperature (θ), and concentration (ϕ) with different values of viscous dissipation parameter i.e., Eckert number (Ec). Ec is the ratio of kinetic energy to thermal energy. Fig. 14 indicates that a weak acceleration in the boundary layer flow is associated with a large rise in viscous dissipation parameter, Ec (values are increased from 0 to 2). The increasing viscous dissipation parameter (Ec) is observed in Fig. 15 to strongly elevate the fluid temperature. With an increase in Ec , the kinetic energy enhances and hence temperature and thermal boundary layer thickness also enhances and as a consequence the greater buoyancy force. Fig. 16 shows that concentration declines slightly.

Figures 17 to 19 depict the evolution in fluid velocity (f'), Jeffery fluid temperature, and concentration (ϕ) with a modification in the chemical reaction parameter (Kr). A first-order chemical reaction, which either destroys or generates the diffusion species, is considered in the present study. $Kr < 0$ causes a generation reaction whereas $Kr > 0$ leads to destruction reaction and causes no reaction for $Kr = 0$. All three cases are studied here. Fig. 17 shows that increasing Kr depletes the velocity magnitudes. Consequently, less flow is induced along the plate resulting in a decrease in the fluid velocity in the boundary layer. The positive values of Kr correspond to destructive reaction and negative values Kr correspond to the generative reaction. Both cases are studied here. Conversely, temperature (Fig. 18) is significantly elevated with increasing Kr effect. Fig. 19 shows that a substantial plummet in concentration is generated with a rise in Kr . The chemical reaction mass diffuses from higher to lower concentration levels. This shows that the diffusion rate can be tremendously altered by chemical reaction.



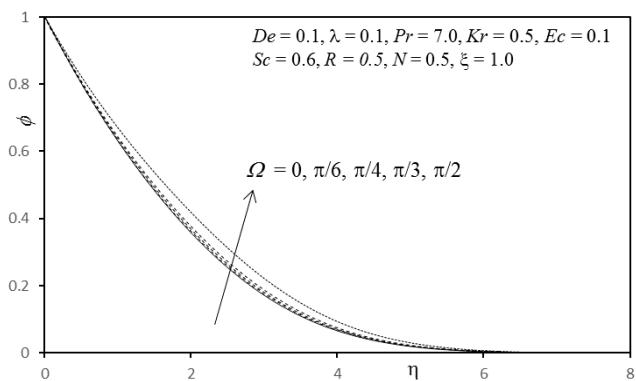


Fig. 10. Influence of Ω on Concentration Profiles

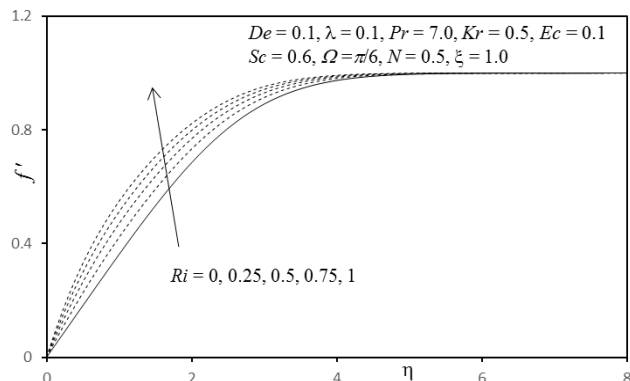


Fig. 11. Influence of Ri on Velocity Profiles

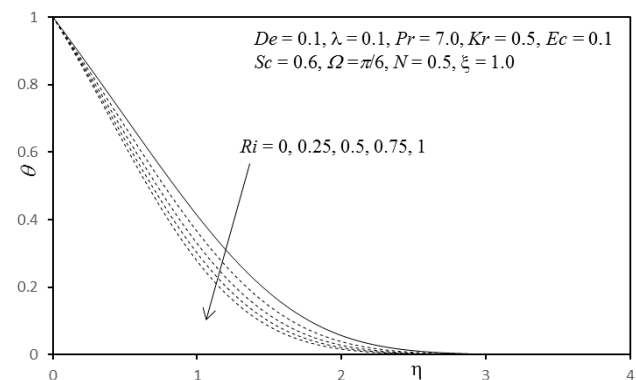


Fig. 12. Influence of Ri on Temperature Profiles

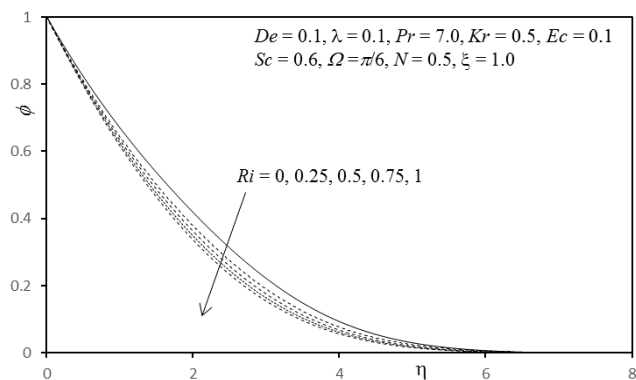


Fig. 13. Influence of Ri on Concentration Profiles

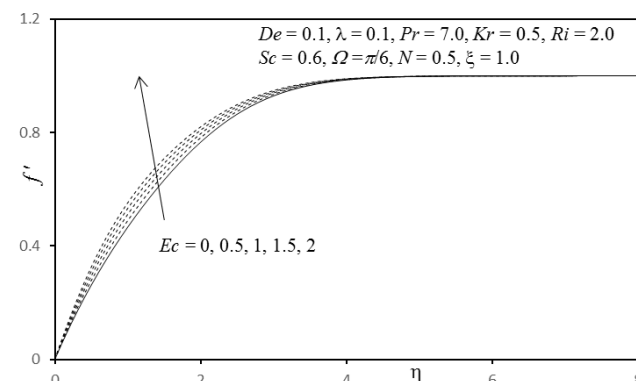


Fig. 14. Influence of Ec on Velocity Profiles

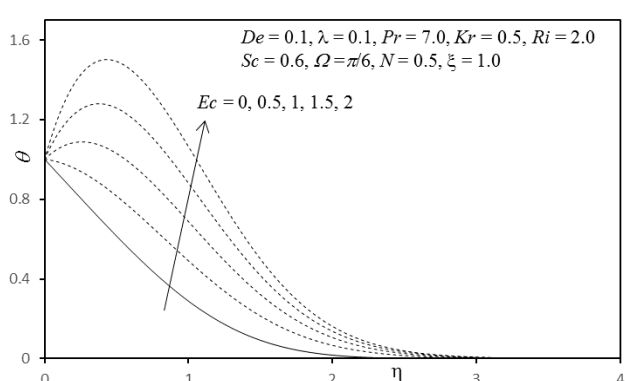


Fig. 15. Influence of Ec on Temperature Profiles

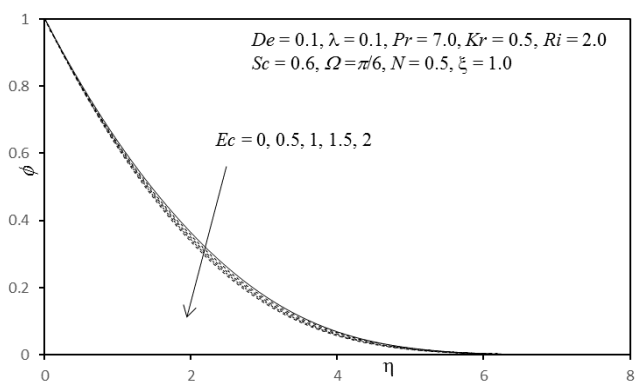


Fig. 16. Influence of Ec on Concentration Profiles

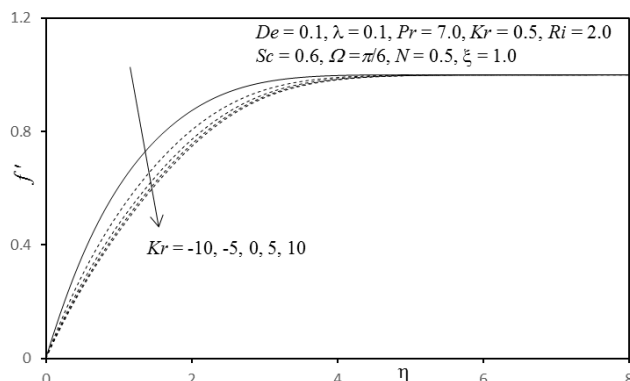


Fig. 17. Influence of Kr on Velocity Profiles



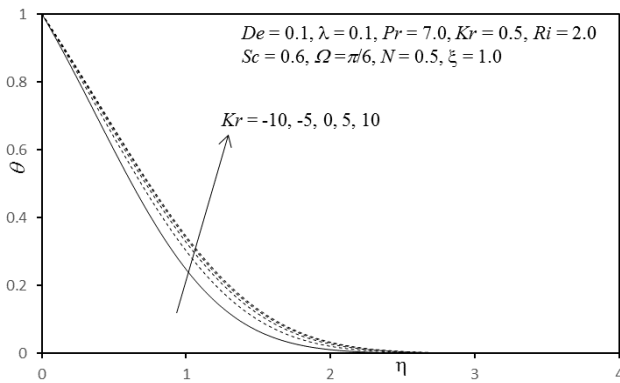


Fig. 18. Influence of Kr on Temperature Profiles

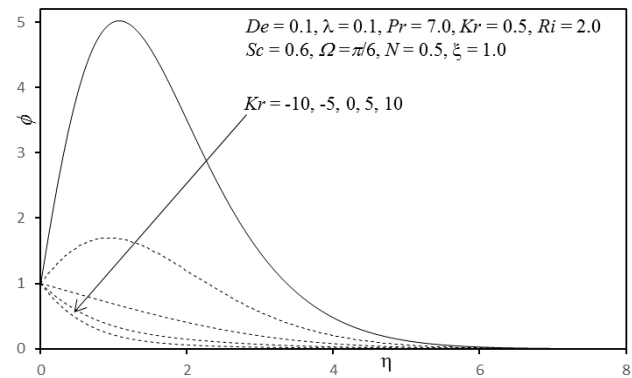


Fig. 19. Influence of Kr on Concentration Profiles

5. Conclusions

A mathematical model was developed to simulate the impacts of the chemical reaction and viscous dissipation in steady-state natural convection boundary layer flow of an electrically-conducting viscoelastic fluid (polymer) from an inclined plate. The governing conservation equations for mass, momentum, energy and concentration and associated wall and free stream boundary conditions were transformed into a nonlinear dimensionless boundary value problem. The Jeffery elastic-viscous model was used. The model was developed to simulate non-Newtonian materials processing. An implicit finite difference scheme (Keller box method) was implemented to solve the partial differential boundary value problem computationally. The main conclusions from the present study may be summarized as follows:

- Velocity was enhanced with increasing Deborah number, relaxation to retardation ratio, Richardson number and Eckert number whereas it was decreased with increasing angle of inclination and chemical reaction parameter.
- The temperature was reduced with increasing Deborah number, relaxation to retardation ratio, Richardson number whereas it was elevated with increasing Eckert number and chemical reaction parameter.
- Concentration was decreased with increasing Deborah number, relaxation to retardation ratio, Richardson number, Eckert number and chemical reaction whereas it was increased with increasing angle of inclination.

In the present study, the transient effects were ignored. These will be considered in the future in addition to alternative rheological models e.g. Oldroyd-B fluid model [46], which is also relevant to thermal polymer processing.

Author Contributions

V. Ramachandra Prasad planned the scheme, initiated the project and suggested the experiments; S. Madhavi conducted the experiments and analyzed the empirical results; S. Abdul Gaffar developed the mathematical modeling and examined the theory validation. The manuscript was written through the contribution of all authors. All authors discussed the results, reviewed and approved the final version of the manuscript.

Acknowledgments

The authors are thankful to DST-WOS-A [Ref: N0. SR/WOS-A/MS-09/2014(G)], New Delhi, for financial support and Management of Madanapalle Institute of Technology and Science, Madanapalle for providing research facilities on the campus.

Conflict of Interest

The authors declared no potential conflicts of interest concerning the research, authorship, and publication of this article.

Funding

The authors received no financial support for the research, authorship, and publication of this article.

Data Availability Statements

The datasets generated and/or analyzed during the current study are available from the corresponding author on reasonable request.



Nomenclature

C	Non-dimensional species concentration	x	Stream wise coordinate
C_f	Skin Friction Coefficient	y	Transverse coordinate
c_p	specific heat	Greek Symbols	
De	Deborah Number	α	Thermal diffusivity
Dm	Mass (species) diffusion	β	Coefficient of thermal expansion
Ec	Eckert number	β^*	Coefficient of species concentration expansion
f	Dimensionless stream function	λ	ratio of relaxation to retardation times
g	Gravitational acceleration	λ_1	retardation time
Gr	Thermal Grashof number	η	Non-dimensional transverse coordinate
k	Thermal conductivity of the fluid	σ	Electric conductivity of the fluid
Kr	Chemical reaction parameter	Ω	Angle of inclination
N	Buoyancy ratio parameter	μ	Dynamic viscosity
Nu	Heat transfer coefficient (Local Nusselt number)	ξ	Non-dimensional tangential coordinate
Pr	Prandtl number	ν	Kinematic viscosity
Ri	Richardson number	θ	Dimensionless temperature
Re	Reynolds number	ρ	Fluid density
S	Cauchy stress tensor	ξ	dimensionless tangential coordinate
Sc	Schmidt number	ψ	Non-dimensional stream function
Sh	Sherwood number	ϕ	Dimensionless concentration
T	Fluid temperature	Subscripts	
V	Velocity vector	w	Conditions on the wall
u, v	Dimensionless velocity components in X and Y direction respectively	∞	Free stream condition

References

- [1] Huang, X. and Gollner M.J., Correlations for evaluation of flame spread over an inclined fuel surface, *Fire Safety Science*, 11, 2014, 222-233.
- [2] Cheng, P., Film condensation along an inclined surface in a porous medium, *International Journal of Heat and Mass Transfer*, 24, 1981, 983-990.
- [3] Anwar Bég, O., Zueco, J., and Chang, T.B., Numerical analysis of hydromagnetic gravity-driven thin-film micropolar flow along an inclined plane, *Chemical Engineering Communications*, 198(3), 2010, 312- 331.
- [4] Balmforth, N.J., Richar V. Craster, Alison c. Rust, Roberto Sassi, Viscoplastic flow over an inclined surface, *J. Non-Newtonian Fluid Mechanics*, 142, 2007, 219-243.
- [5] Ashraf, M.B., Hayat, T., Alsaedi, A., Radiative mixed convection flow of an Oldroyd-B fluid over an inclined stretching surface, *Journal of Applied Mechanics and Technical Physics*, 57, 2016, 317–325.
- [6] Pruess, K., Zhang, Y., A hybrid semi-analytical and numerical method for modeling wellbore heat transmission, *Proc. 30th Workshop on Geothermal Reservoir Engineering, Stanford University, Stanford, California, USA, 2005.*
- [7] Greener, Y., and Middleman, S., Blade-coating of a viscoelastic fluid, *Polymer Engineering and Science*, 14, 1974, 791-796.
- [8] Chang, H.C., Demekhin, E. A., *Complex Wave Dynamics on Thin Films*, Elsevier, Amsterdam, 2002.
- [9] Johnson, A.F., Rheology of thermoplastic composites I, *Composites Manufacturing*, 6, 1995, 153-160.
- [10] Nepal C. Roy, Md. Anwar Hossain, Rama Subba Reddy Gorla, Combustible Boundary-Layer Flows Along Inclined Hot Surfaces with Streamwise Surface Temperature Variations, *Journal of Thermophysics and Heat Transfer*, 33(1), 2019. <https://doi.org/10.2514/1.T5465>
- [11] Sulochana, C., Ashwinkumar, G.P., Sandeep, N., Effect of frictional heating on mixed convection flow of chemically reacting radiative Casson nanofluid over an inclined porous plate, *Alexandria Engineering Journal*, 27(4), 2018, 2573-2584. <https://doi.org/10.1016/j.aej.2017.08.006>
- [12] Hayat, T., Muhammed Ijaz Khan, Muhammad Waqas, Ahmed Alsaedi, On Cattaneo-Christov heat flux in the flow of variable thermal conductivity Eyring-Powell fluid, *Results in Physics*, 7, 2017, 446-450.
- [13] Hayat, T., Ijaz Khan, M., Farooq, M., Tabassam Yasmeen, Alsaedi, A., Stagnation point flow with Cattaneo-Christov heat flux and homogeneous-heterogeneous reactions, *Journal of Molecular Liquids*, 220, 2016, 49-55.
- [14] Muhammed Ijaz Khan, Muhammad Waqas, T. Hayat, Ahmed Alsaedi, A comparative study of Casson Fluid with homogeneous-heterogeneous reactions, *Journal of Colloid and Interface Science*, 498, 2017, 85-90.
- [15] RamReddy, Ch., Naveen, P., Srinivasacharya, D., Influence of Non-linear Boussinesq Approximation on Natural Convective Flow of a Power-Law Fluid along an Inclined Plate under Convective Thermal Boundary Condition, *Nonlinear Engineering*, 8(1), 2018, 94-106.
- [16] RamReddy, Ch., Naveen, P., Srinivasacharya, D., Nonlinear Convective Flow of Non-Newtonian Fluid over an Inclined Plate with Convective Surface Condition: A Darcy–Forchheimer Model, *Int. J. Appl. Comput. Math.*, 4, 2018, 51.



- [17] RamReddy, Ch., Naveen, P., Srinivasacharya, D., Quadratic Convective Flow of a Micropolar Fluid along an Inclined Plate in a Non-Darcy Porous Medium with Convective Boundary Condition, *Nonlinear Engineering*, 6(2), 2017, 139-151.
- [18] Manzoor, N., Maqbool, K., Anwar Bég, O., Shaheen, S., Adomian decomposition solution for propulsion of dissipative magnetic Jeffrey biofluid in a ciliated channel containing a porous medium with forced convection heat transfer, *Heat Transfer - Asian Research*, 48(2), 2018, 556-581.
- [19] Prasad, V.R., Abdul Gaffar, S., Keshava Reddy, E., Anwar Bég, O., Numerical study of non-Newtonian boundary layer flow of Jeffreys fluid past a vertical porous plate in a non-Darcy porous medium, *Int. J. Comp. Meth. Engineering Science & Mechanics*, 15(4), 2014, 372-389.
- [20] Abdul Gaffar, S., Ramachandra Prasad, V., Anwar Bég, O., Hidayathullah Khan, Md., Venkatadri, K., Effects of ramped wall temperature and concentration on viscoelastic Jeffrey's fluid flows from a vertical permeable cone, *J. Brazilian Soc. Mech Sci. Eng.*, 40, 2018, 441-459.
- [21] Kumar, M., Reddy, G.J., Dalir N., Transient entropy analysis of the magnetohydrodynamics flow of a Jeffrey fluid past an isothermal vertical flat plate, *Pramana*, 91, 2018, 60.
- [22] Shukla, N., Puneet Rana, Anwar Bég, O., Kadir, A., Bani Singh, Unsteady electromagnetic radiative nanofluid stagnation point flow from a stretching sheet with chemically reactive nanoparticles, Stefan blowing effect and entropy generation, *Proc. IMechE: Part N-Journal of Nanomaterials, Nanoengineering, and Nanosystems*, 232(2-3), 2018, 69-82.
- [23] Ijaz Khan, M., Qayyum, S., Hayat, T., Waqas, M., Imran Khan, M., Alsaedi, A., Entropy generation minimization and binary chemical reaction with Arrhenius activation energy in MHD radiative flow of nanomaterial, *J. Mol. Liq.*, 259, 2018, 274-283.
- [24] Mondal, H., Pal, D., Chatterjee, S., Sibanda, P., Thermophoresis and Soret-Dufour on MHD mixed convection mass transfer over an inclined plate with non-uniform heat source/sink and chemical reaction, *Ain Shams Engineering Journal*, 9(4), 2018, 2111-2121.
- [25] Krishnamurthy, M.R., Prasannakumara, B.C., Gireesha, B.J., Rama Subba Reddy Gorla, Effect of chemical reaction on MHD boundary layer flow and melting heat transfer of Williamson nanofluid in porous medium, *Engg. Sci. and Tech., an Int. J.*, 19(1), 2016, 53-61.
- [26] Ramana Reddy, J.V., Sugunamma, V., Sandeep, N., Sulochana, C., Influence of chemical reaction, radiation and rotation on MHD nanofluid flow past a permeable flat plate in porous medium, *Journal of the Nigerian Mathematical Society*, 35(1), 2016, 48-65.
- [27] Ijaz Khan, M., Hayat, T., Imran Khan, M., Alsaedi, A., Activation energy impact in nonlinear radiative stagnation point flow of Cross Nanofluid, *Int. Comm. in Heat and Mass Transfer*, 91, 2018, 216-224.
- [28] Hayat, T., Ijaz Khan, M., Qayyum, S., Alsaedi, A., Entropy generation in flow with silver and copper nanoparticles, *Colloids and Surfaces A: Physicochemical and Engineering Aspects*, 539, 2018, 335-346.
- [29] Hayat, T., Qayyum, S., Ijaz Khan, M., Alsaedi, A., Entropy generation in magnetohydrodynamic radiative flow due to rotating disk in presence of viscous dissipation and Joule heating, *Physics of Fluids*, 30, 2018, 017101.
- [30] Ahmed Khan, W., Ijaz Khan, M., Hayat, M., Alsaedi, A., Entropy generation minimization (EGM) of nanofluid flow by a thin moving needle with nonlinear thermal radiation, *Physica B: Condensed Matter*, 534, 2018, 113-119.
- [31] Hayat, T., Ijaz Khan, M., Qayyum, S., Alsaedi, A., Modern developments about the statistical declaration and probable error for skin friction and Nusselt number with copper and silver nanoparticles, *Chinese Journal of Physics*, 55(6), 2017, 2501-2513.
- [32] Ijaz Khan, M., Waqas, M., Hayat, T., Imran Khan, M., Alsaedi, A., Numerical simulation of nonlinear thermal radiation and homogeneous-heterogeneous reaction in convective flow by a variable thickened surface, *Journal of Molecular Liquids*, 246, 2017, 259-267.
- [33] Hayat, T., Khan, M., Khan, M.I., Alsaedi, A., Ayub, M., Electromagneto squeezing rotational flow of Carbon (C)-Water (H₂O) kerosene oil nanofluid past a Riga plate: A numerical study, *PLoS ONE*, 12(8), 2017, e0180976.
- [34] Ijaz Khan, M., Qayyum, S., Hayat, T., Imran Khan, M., Alsaedi, A., Ahamd Khan, T., Entropy generation in radiative motion of tangent hyperbolic nanofluid in presence of activation energy and nonlinear mixed convection, *Physics Letters A*, 382(31), 2018, 2017-2026.
- [35] Abdul Gaffar, S., Ramachandra Prasad, V., Keshava Reddy, E., MHD free convection flow of non-Newtonian Eyring-Powell fluid from vertical surface in porous media with Hall/Ionslip currents and Ohmic dissipation, *Alexandria Engineering Journal*, 55, 2016, 875-905.
- [36] Abdul Gaffar, S., Ramachandra Prasad, V., Keshava Reddy, E., Computational Study of MHD free convection flow of non-Newtonian Tangent Hyperbolic fluid from a vertical surface in porous media with Hall/Ionslip current and Ohmic dissipation, *International Journal of Applied and Computational Mathematics*, 3(2), 2017, 859-890.
- [37] Anwar Beg, O., Abdul Gaffar, S., Ramachandra Prasad, V., Uddin, M.J., Computational solutions for non-isothermal, nonlinear magnetoconvection in porous media with hall/ionslip currents and ohmic dissipation, *Engineering Science and Technology, an International Journal*, 19(1), 2016, 377-394.
- [38] Maceiras, A., and Martins, P., High-temperature polymer-based magnetoelectric nanocomposites, *European Polymer Journal*, 64, 2015, 224-228.
- [39] Xulu, P.M., Filipcsei, P., Zrinyi, M., Preparation and responsive properties of magnetically soft poly (*N*-isopropyl acrylamide) gels, *Macromolecules*, 33(5), 2000, 1716-1719.
- [40] Anwar Bég, O., *Numerical methods for multi-physical magnetohydrodynamics*, Chapter 1, pp. 1-112, New Developments



- in Hydrodynamics Research, M. J. Ibragimov and M. A. Anisimov, Eds., Nova Science, New York, 2012.
- [41] Hayat, T., Alsaedi, A., Shehzad, S.A., Three dimensional flow of Jefferys fluid with convective surface boundary conditions, *Int. J. Heat & Mass Transfer*, 55, 2012, 3971-3976.
- [42] M.T. Shaw, *Introduction to Polymer Rheology*, Wiley, New York, 2012.
- [43] Abdul Gaffar, S., Anwar Beg, O., Prasad, V.R., Mathematical Modelling of Natural Convection in a Thrid-Grade viscoelastic micropolar fluid from an isothermal inverted cone, *Iranian Journal of Science and Technology, Transactions of Mechanical Engineering*, 2018. <https://doi.org/10.1007/s40997-018-0262-x>
- [44] Gaffar, S.A., Prasad, V.R., Kumar, B.R., Anwar Bég, O., Computational modeling and solutions for mixed convection boundary layer flows of nanofluid from a non-isothermal wedge, *Journal of Nanofluids*, 7, 2018, 1–9.
- [45] Lloyd, J.R., Sparrow, E.M., Combined forced and free convection flow on vertical surfaces, *International Journal Heat & Mass Transfer*, 13(2), 1970, 434-438.
- [46] Norouzi, M., Davoodi, M., Anwar Bég, O., Shamshuddin, MD., Theoretical study of Oldroyd-B viscoelastic fluid flow through curved pipes with slip effects in polymer flow processing, *Int. J. Applied Computational Mathematics*, 4, 2018, 108.

ORCID iD

Santhosh Madhavi  <https://orcid.org/0000-0002-5722-9792>

V. Ramachandra Prasad  <http://orcid.org/0000-0002-9168-3825>

Shaik Abdul Gaffar  <http://orcid.org/0000-0002-7368-1658>



© 2022 Shahid Chamran University of Ahvaz, Ahvaz, Iran. This article is an open access article distributed under the terms and conditions of the Creative Commons Attribution-NonCommercial 4.0 International (CC BY-NC 4.0 license) (<http://creativecommons.org/licenses/by-nc/4.0/>).

How to cite this article: Madhavi S., Ramachandra Prasad V., Abdul Gaffar S. Polymeric Dissipative Convection Flow from an Inclined Plane with Chemical Reaction: Numerical Study, *J. Appl. Comput. Mech.*, 8(2), 2022, 416–428. <https://doi.org/10.22055/JACM.2019.30582.1747>

Publisher's Note Shahid Chamran University of Ahvaz remains neutral with regard to jurisdictional claims in published maps and institutional affiliations.

